Global bifurcations and bistability at the locking boundaries of a semiconductor laser with phase-conjugate feedback

Kirk Green and Bernd Krauskopf
Department of Engineering Mathematics, University of Bristol, Bristol BS8 1TR, UK
(Dated: February 4, 2002)

We investigate dynamics and bifurcations of a single-mode semiconductor laser subject to phase-conjugate feedback near the locking region. The system is described by rate equations which are a three-dimensional system with a delay. With new tools that go much beyond mere simulation, we find and follow steady states regardless of their stability and compute unstable manifolds of saddle points. Furthermore, we identify heteroclinic bifurcations, which turn out to be responsible for bistability and excitability at the locking boundaries.

I. INTRODUCTION

Recently there has been much interest in the nonlinear dynamics of semiconductor lasers; see, for example, the recent overviews Refs. [1, 2] and further references therein. Due to the material properties of semiconductor lasers, external influences can alter the stability and dynamics of the laser dramatically. Knowledge of this effect is therefore essential for physical applications. Of particular interest are lasers subject to optical feedback, such as lasers with conventional optical feedback (COF) from an external mirror [3, 4], lasers with phase conjugate feedback [5–10], the case considered here, lasers with opto-electronic feedback [11], and mutually coupled lasers with delay [12]. In all these cases the relevant and generally well-established models are delay differential equations (DDEs) [13].

Delay differential equations have received a lot of attention recently. Other areas where DDEs are crucial include biology [14], neural networks [15] and control theory [16]. It is quite a challenge to understand the dynamics and bifurcations of a DDE. Already in the case of one fixed delay τ (like in a laser with feedback), the phase space of the DDE is the infinite-dimensional space of continuous functions on the delay interval $[-\tau, 0]$; see Ref. [20]. Tackling delay equations arising in applications is analytically very hard, and for a long time the only numerical tool was direct simulation by integration of the DDE. Very recently the package DDE-BIFTOOL [23] was developed, allowing numerical continuation of steady states and periodic solutions and the detection of their local bifurcations. Building on this work, we developed a method for computing unstable manifolds in DDEs. These new tools allow one to find global bifurcations that are responsible for sudden changes of the observed dynamics of a DDE.

In this paper we bring these new tools to bear to study the locking mechanism in a semiconductor laser receiving *phase-conjugate feedback* (PCF) from a phase-conjugating mirror (PCM) [7, 9, 10]. Phase-conjugate feedback is physically interesting as it produces a return wave that coincides exactly with the incident wave, so that alignment is less of an issue. Furthermore, distortions are undone on the return trip in the external cavity. A laser with PCF was shown to exhibit complicated nonlinear dynamics, including stable periodic operation, quasiperiodic motion and chaos, as was found in detailed simulations of bifurcation diagrams, phase plots and optical spectra. The overall picture is that of regions of periodic output that are interspersed with 'bubbles' of chaos [9, 10].

Here we concentrate on the mechanism of locking. Physically, in its locking range the PCF laser is both frequency locked and phase locked to the frequency of the PCM pump laser. Unlike the case of a COF laser, phase locking in a PCF laser does not depend on the feedback phase. In particular, phase locking results in an ultra-narrow laser line-width which has been shown to be stable even with the addition of noise [9]. By continuing steady states and computing the unstable manifolds of saddle points we find that hysteresis loops and global bifurcations are involved in the mechanism of locking in the PCF laser.

II. RATE EQUATIONS

Our object of study is a single-mode PCF laser receiving feedback from a PCM which responds instantaneously. The rate equations describing this PCF laser are well established [7, 9, 10] and can be written as

$$\begin{aligned} \frac{dE}{dt} &= \frac{1}{2}\left[-i\alpha G_N(N(t)-N_{\rm sol}) + \left(G - \frac{1}{\tau_p}\right)\right]E(t) \\ &+ \kappa E^*(t-\tau)\exp[i\phi_{\rm PCM}] \\ \frac{dN}{dt} &= \frac{I}{q} - \frac{N(t)}{\tau_e} - G\,|E(t)|^2 \end{aligned} \tag{1}$$

for the evolution of the slowly varying complex electric field $E(t) = E_x(t) + iE_y(t)$ and the population inversion $N(t)$. In system (1), nonlinear gain is included as $G = G_N(N - N_0)(1 - \epsilon P)$, where $\epsilon = 3.57 \times 10^{-8}$ is the nonlinear gain coefficient and $P = |E(t)|^2$ is the intensity. This produces an effective detuning of 166 MHz. Parameter values are set to realistic values [10], namely the line-width enhancement factor $\alpha = 3$, the optical gain $G_N = 1190\ \mathrm{s}^{-1}$, the photon lifetime $\tau_p = 1.4$ ps,

the injection current $I = 65.1$ mA, the magnitude of the electron charge $q = 1.6 \times 10^{-19}$ C, the electron lifetime $\tau_e = 2$ ns, and the transparency electron number $N_0 = 1.64 \times 10^8$. The phase shift $\phi_{\rm PCM}$ at the PCM was set to zero and $N_{\rm sol} = N_0 + 1/(G_N \tau_p)$. The feedback term in system (1) involves the feedback rate κ and the external cavity round-trip time τ which we fix at $\tau = 2/3$ ns. Together they form the dimensionless bifurcation parameter $\kappa\tau$.

System (1) is written in the frame of reference of the solitary laser. A locked solution is one where the frequency of the PCM pump laser is locked to that of the solitary laser and, therefore, locked solutions are steady states of system (1). Note that noise terms due to spontaneous emission have been left off system (1). It has been shown that both intensity and frequency noise are negligible at the low frequency range we are dealing with [7].

Mathematically, system (1) is a system of DDEs [20]. The state of the system at time $t > 0$ is a continuous function on the time interval $[t - \tau, t]$, which is an evolution of the initial condition defined on the time interval $[-\tau, 0]$. Therefore, the system is infinite-dimensional. While (E, N)-space is not the phase space of system (1), it is nevertheless helpful to show the dynamics projected onto (E, N)-space, which is also called the physical space of system (1).

System (1) is symmetric under the transformation $E \to -E$, which corresponds to a rotation of π of the E-plane, so that an attractor is either symmetric, or has a symmetric counterpart [10, 21]. Physically, this symmetry corresponds to a phase shift by π. The symmetry implies restrictions on the types of bifurcations of periodic solutions: for example, symmetric periodic solutions cannot undergo period-doubling bifurcations [22]. More generally, this discrete symmetry allows for the possibility of symmetry-breaking bifurcations. Note that the PCF laser considered here is different from the COF laser in terms of the underlying symmetry of the governing equations [21]. The COF laser is symmetric under any rotation of the electric field E and does not feature symmetry breaking bifurcations.

III. COMPUTATIONAL METHODS FOR DDEs

In our study we make use of very recent developments in theory and numerical methods for DDEs. In simulations we integrate system (1) with an Adams-Bashforth forth-order multistep method [19]. Moreover, we use recently developed tools for DDEs that go beyond simulation.

First, we use the continuation package DDE-BIFTOOL [23], consisting of Matlab routines, for the bifurcation analysis of steady states and periodic solutions. This not only allows one to find and follow stable solutions (those one also finds by simulation), but also unstable ones. Furthermore, DDE-BIFTOOL detects local

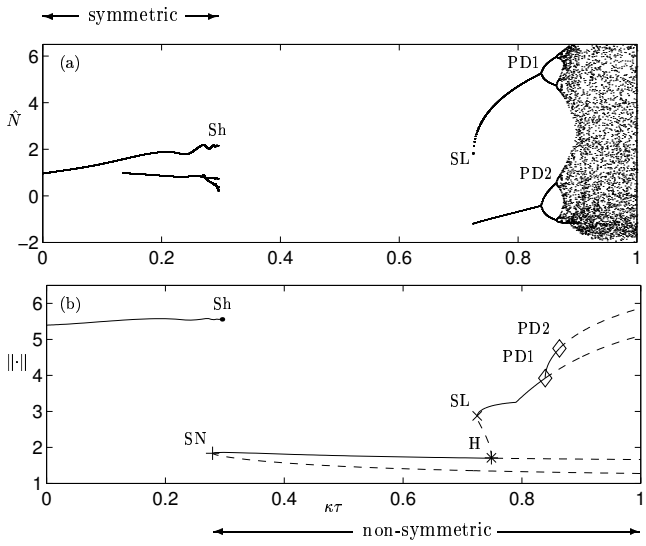

FIG. 1: Bifurcation diagram obtained by simulation showing normalized inversion $\hat{N}$ versus the feedback strength $\kappa\tau$ (a), and computed with DDE-BIFTOOL showing a normalized amplitude versus $\kappa\tau$ (b); see text for details.

bifurcations, including saddle-node bifurcations, Hopf bifurcations, period-doubling bifurcations and saddle-node bifurcations of limit cycles. The continuation of bifurcations leading to mixed-mode oscillations of a COF laser in Ref. [17] and our bifurcation analysis of the PCF laser here and in Ref. [18] are first examples of continuation studies with DDE-BIFTOOL.

Second, we compute the one-dimensional (1D) unstable manifolds of saddle steady states with one unstable eigenvalue. Each 1D unstable manifold has two branches, which are computed by integrating from two initial condition along the associated 1D unstable eigendirection close to but on different sides of the steady state. This eigendirection can be found by an iterative approach [19] or with a new routine that was recently added to DDE-BIFTOOL. Knowing at which attractor the branches of 1D unstable manifolds end up is crucial for understanding the global dynamics, as will become clear in Section V.

IV. BIFURCATION DIAGRAMS

Figure 1 contains two bifurcation diagrams. In Fig. 1(a) we integrated system (1) and plotted (after transients died away) the normalized value of the inversion $\hat{N} = (N/N_{sol} - 1) \times 10^3$ whenever the intensity P crossed its average value in the positive direction [10]. No points in the bifurcation diagram correspond to a locked solution. A small number of points correspond to a periodic solution. A large number of points correspond to quasiperiodic or chaotic dynamics. Due to the presence of hysteresis discussed below, the periodic solution for

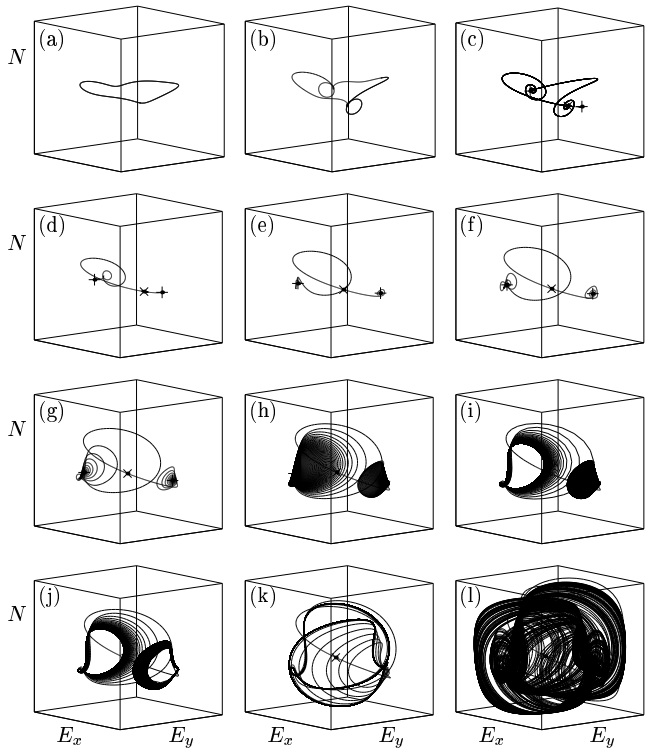

FIG. 2: Phase portraits shown in projection onto (E, N)-space; the box is $[-200,\ 200]\times[-200,\ 200]\times[7.61\times10^8,\ 7.68\times10^8]$. From (a) to (l), $\kappa\tau$ takes the values 0.1000, 0.2700, 0.2952, 0.3065, 0.4410, 0.5180, 0.6182, 0.7183, 0.7252, 0.7253, 0.7904, and 0.9004. Except for (a) and (b), plotted are both branches of the 1D unstable manifold of one of the two symmetric saddle points ($\times$).

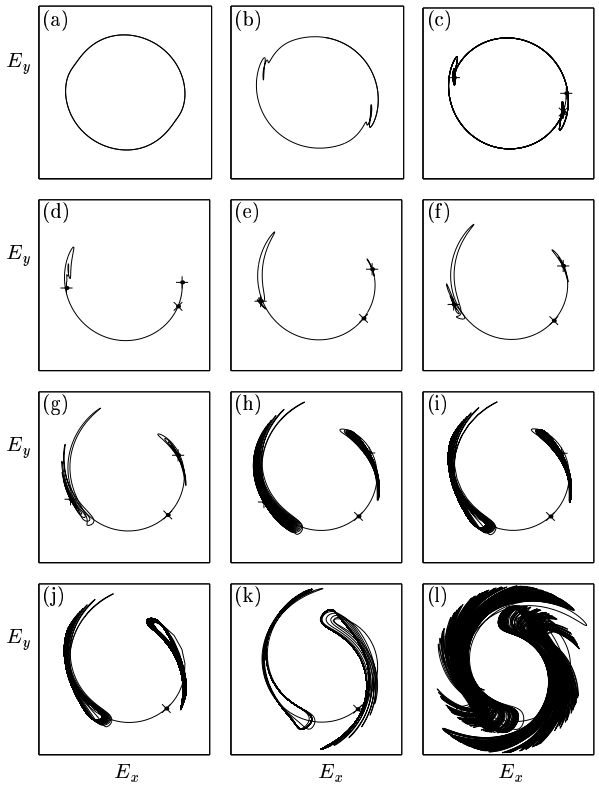

FIG. 3: Projection of plots in Fig. 2 onto the E-plane; the square is $[-270,\ 270]\times[-270,\ 270]$.

$\kappa\tau \in [0.0000,\ 0.2953]$ was computed for increasing $\kappa\tau$, while the periodic solution for $\kappa\tau \in [0.7487,\ 0.9004]$ was computed for decreasing $\kappa\tau$.

Figure 1(b) was obtained with DDE-BIFTOOL. For steady states we plot $Re(E)$ and for periodic solutions we plot $|\max(Re(E)) - \min(Re(E))|$, offset by the $Re(E)$-value of the steady states at the Hopf point. Attracting solutions are drawn as solid curves, while unstable solutions are drawn as dashed curves. By studying the eigenvalues of the system we are able to identify the bifurcations involved, namely a saddle-node bifurcation *SN*, a Hopf bifurcation *H*, period-doubling bifurcations *PD1* and *PD2* and a saddle-node bifurcation of limit cycles *SL*. A global Shil'nikov bifurcation *Sh* was observed at $\kappa\tau \approx 0.2953$. The symmetry of solution branches, which can be found from the respective phase portraits, is indicated at the top and bottom of Figure 1.

Figure 1(a) is useful for investigating bifurcations of attractors, but in Fig. 1(b) we also follow unstable solutions and their bifurcations. We can already see that the system features hysteresis at the boundaries of the locking region, which is discussed in more detail below. Figure 1(b) also shows that the extra branches that develop in Fig. 1(a) at $\kappa\tau \geq 0.1347$ are not bifurcations. They are due to the symmetric limit cycle spiraling through, and thus producing extra crossings with, its value of average intensity.

V. UNSTABLE MANIFOLDS

Figures 2 and 3 show the phase portraits corresponding to Fig. 1 in projection onto (E, N)-space [Fig. 2] and the E-plane [Fig. 3]. Except for panels (a) and (b), which were obtained by simulation, these phase portraits were obtained by plotting both branches of the 1D unstable manifold of one of the two symmetric saddle points, marked by $\times$; the corresponding attracting steady states are marked by $+$. The bifurcation diagrams in Fig. 1, along with Figs. 2 and 3, present a complete picture of the route into and out of locking for the PCF laser specified in Section II.

For very low values of $\kappa\tau$, system (1) has an almost planar periodic solution surrounding the origin of the E-plane [Figs. 2, 3 (a)], which is the continuation of the free-running laser ($\kappa\tau = 0$) that has constant power and inversion. With increasing feedback the laser is destabilized. First, the periodic solution starts to curl up near

two distinct points [Figs. 2, 3 (b)]. It develops a typical shape and does end in a Shil'nikov bifurcation *Sh* when it hits two saddle-focus steady states at $\kappa\tau \approx 0.2953$, [Fig. 1(b)]. The exact nature of this global bifurcation is detailed in Sec. VI A. The two saddle-focus steady states are each others symmetric counter parts and are born together with two attractors in the saddle-node bifurcation *SN* at $\kappa\tau \approx 0.2794$, that is, before the Shil'nikov bifurcation [Fig. 1(b)]. This produces a region of bistability between the pair of attracting steady states and the periodic solution. Indeed, for $\kappa\tau \in [0.2794, 0.2953]$ one branch of the 1D unstable manifold converges to the periodic solution, while the other branch converges to a locked steady state [Figs. 2, 3 (c)]. Physically this bistability means that the laser is capable of producing locked or periodic output for the same experimental value of $\kappa\tau$, depending on the initial condition. After the Shil'nikov bifurcation, bistability is lost and both branches of the saddle-focus steady state converge to one of the two locked solutions, which are the only attractors and symmetric images of each other [Figs. 2, 3 (d)].

This bistability leads to a hysteresis loop: for increasing $\kappa\tau$ the symmetric periodic solution is destroyed in the Shil'nikov bifurcation and the system jumps to one of the steady states, whereas for decreasing $\kappa\tau$ the two steady states are destroyed in the saddle-node bifurcation and the system jumps to the symmetric periodic solution. So not only do we see a qualitative change in the attracting solutions, but we also see a change in the symmetry of the attractor, as is indicated in Fig. 1.

As $\kappa\tau$ is increased further through the locking region, the two branches of the 1D manifold of the saddle steady state continue to converge to the respective locked solutions, but with an increasingly larger degree of spiraling [Figs. 2, 3 (e)(f)(g)(h)]. Physically this spiraling corresponds to the characteristic relaxation oscillations of the laser (a periodic exchange of energy between electric field and inversion), which is still damped. At $\kappa\tau \approx 0.7247$ there is a saddle-node bifurcation of limit cycles *SL* creating two pairs of symmetric periodic solutions [Fig. 1(b)], one attracting and one of saddle-type. The attracting periodic solutions grow at a rate proportional to $\sqrt{\kappa\tau}$, one speaks of an undamping of the relaxation oscillations. The saddle periodic solutions shrink down to the locked steady state and disappear in a sub-critical Hopf bifurcation *H* at $\kappa\tau \approx 0.7487$; see [Fig. 1(b)]. This bifurcation results in the loss of stability of the locked steady states and forms the boundary of the locking range. The system jumps to one of the two attracting periodic solutions and the laser produces self-pulsations (relaxation oscillations). Indeed both branches of the unstable manifold of the saddle steady state end up at an attracting periodic solution [Figs. 2, 3 (j)].

In other words, also the right-hand locking boundary is associated with a region of bistability: for $\kappa\tau \in [0.7247, 0.7487]$ both the pair of locked solutions as well as the pair of periodic solutions corresponding to undamped relaxation oscillations are stable. Again, this leads to a

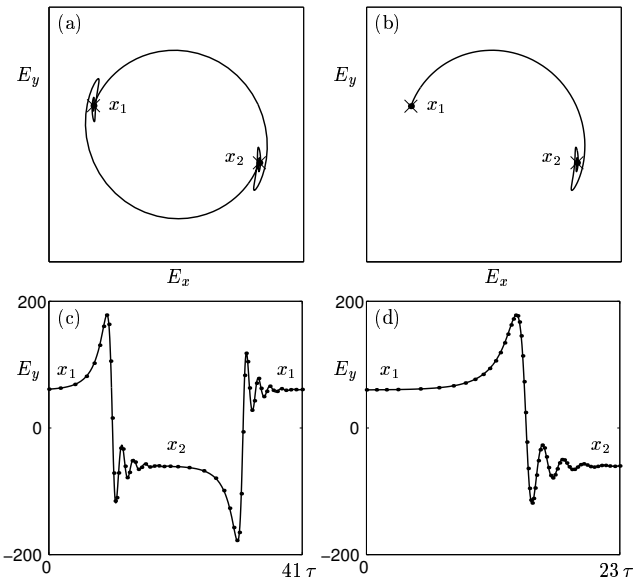

FIG. 4: The periodic solution just before the Shil'nikov bifurcation (a) and the heteroclinic connection between the saddle steady states x_1 and x_2 at the Shil'nikov bifurcation (b). Panels (c) and (d) show the corresponding time-traces of E_y with the mesh points highlighted.

hysteresis loop when $\kappa\tau$ is swept up and down through *SL* and *H*.

Note already that the two branches of the unstable manifold of the saddle steady state behave differently just after *SL* [Figs. 2, 3 (h)] and just before *H* [Figs. 2, 3 (i)]. As will be discussed in detail in Section VI B, this implies the existence of a heteroclinic bifurcation between *SL* and *H*.

When $\kappa\tau$ is increased further, the pair of stable periodic solutions undergoes a period-doubling cascade starting at $\kappa\tau \approx 0.8393$ [Fig. 1(b)]. This eventually leads to both branches of the 1D unstable manifold of the saddle steady state accumulating on a chaotic attractor [Figs. 2, 3 (l)]. Eventually the two attractors collide in an attractor crisis caused by a collision of their basins of attraction, culminating in symmetry restoring inside the chaotic region [10].

VI. GLOBAL BIFURCATIONS

We already mentioned in the last section that at both boundaries of the locking range we find global bifurcations, namely a Shil'nikov bifurcation at the left-hand boundary and a heteroclinic bifurcation between a saddle steady state and a saddle periodic solution at the right-hand boundary. We now discuss these two global bifurcations in detail.

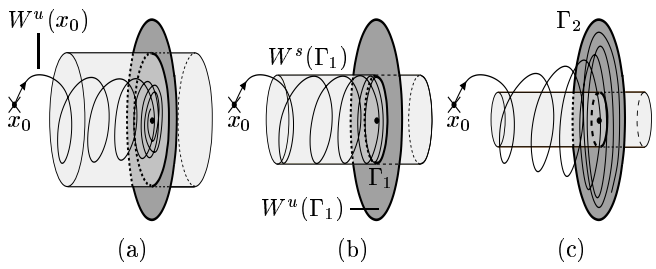

FIG. 5: Before (a), at (b) and after (c) a heteroclinic connection between a saddle steady state x_0 and a saddle periodic solution Γ_1.

A. Shil'nikov bifurcation

In Figure 4 (a) we show the symmetric limit cycle just before the Shil'nikov bifurcation *Sh* in which it hits the pair of saddle steady states x_1 and x_2. A time-trace of E_y over its period $\mathsf{T} \approx 41.0\tau$ is shown in Figure 4 (c), where the mesh points used in the DDE-BIFTOOL continuation are highlighted. When approaching *Sh* the period T goes to infinity. At *Sh* the periodic solution disappears and instead we have a symmetric pair of heteroclinic connections between x_1 and x_2, one of which is shown in Figure 4 (b). This connecting orbit was computed with the new extension of DDE-BIFTOOL introduced in Ref. [24]. Its time-trace with highlighted mesh points is shown in Figure 4 (d). An analysis of the eigenvalues of the saddle-foci shows a negative saddle quantity, implying that there is a unique stable limit cycle involved in the Shil'nikov bifurcation [22].

The fact that the Shil'nikov bifurcation appears as two simultaneous heteroclinic connections is due to the symmetry of Eqs. (1). When one divides out the symmetry and identifies x_1 and x_2 then one gets just a regular homoclinic connection at the Shil'nikov bifurcation.

We remark that after but near the Shil'nikov bifurcation *Sh* the system is excitable — an example of excitability due to a heteroclinic bifurcation [25]. When the locked solution is perturbed to the other-side of the saddle steady state it will produce a large excursion by following roughly the old heteroclinic connection and ending up at the other locked solution [Fig. 2, 3 (d)]. Physically, this corresponds to a phase jump by π and a relaxing pulse in the power of the laser. We remark that the amplitude of this pulse is quite small. This can also be inferred from Fig. 3 (d): the distance from the origin in the E-plane does not change much and the power is the square of this distance.

B. Heteroclinic connection

Between the saddle-node bifurcation *SL* and the Hopf bifurcation *H* we have another region of bistability where again the laser can produce qualitatively different stable output depending on the initial condition. The infinite-dimensional stable manifold of the unstable periodic solution forms the boundary between solutions converging to the locked steady state or the stable periodic solution.

As the unstable periodic solution decreases in size there must be a heteroclinic bifurcation between the two attractors, and we explain this in detail now. Figures 2, 3 (i) show the 1D unstable manifolds for $\kappa\tau = 0.7252$, which is typical of the region $\kappa\tau \in [0.7247, 0.7252]$ where we see one branch spiraling into a periodic solution, while the other branch spirals to a locked solution. However, at $\kappa\tau = 0.7253$ [Figs. 2, 3 (j)], one branch spirals into a periodic solution as before, but the other branch now spirals out to the symmetric counterpart of this periodic solution. This implies that between the values of $\kappa\tau = 0.7252$ and $\kappa\tau = 0.7253$ a heteroclinic bifurcation must take place, as is sketched in Fig. 5. Initially, the 1D unstable manifold $W^u(x_0)$ of x_0 spirals into the locked solution [Fig. 5(a)]. As $\kappa\tau$ is increased the amplitude of the saddle periodic solution Γ_1 starts to decrease, from maximum amplitude at *SL* to zero amplitude at *H*, as can be seen in Fig. 1(b). For a particular value of $\kappa\tau$, $W^u(x_0)$ forms a connection with the stable manifold $W^s(\Gamma_1)$ of the saddle periodic solution Γ_1 [Fig. 5(b)]. As $\kappa\tau$ is increased further this connection is lost and $W^u(x_0)$ spirals out to the attracting periodic solution Γ_2 [Fig. 5(c)]. This behaviour is preserved after the sub-critical Hopf bifurcation *H*: one branch of the saddle steady state converges to a stable periodic solution and the other branch converges to the symmetric counterpart of this periodic solution [Figs. 2, 3 (k)].

VII. DISCUSSION

We studied in detail the transitions into and out of locking of a semiconductor laser with phase-conjugate feedback. Both feature bistabilities leading to hysteresis loops. Furthermore, both transitions to locking are associated with global bifurcations, namely a Shil'nikov bifurcation and heteroclinic bifurcation between a steady state and a periodic solution, respectively. New tools for DDEs allowed us to study these global bifurcations in unprecedented detail.

The bifurcation scenario we described is structurally stable. Initial investigations of some bifurcation curves in the plane of $\kappa\tau$ versus injection current indicate that this scenario appears to be typical for a PCF laser pumped near its threshold current (up to about 7.7% above threshold), which is the region of injection current most commonly investigated in feedback experiments. The construction of a full two-dimensional bifurcation diagram is the next logical step. However, at present this is quite a challenge and requires further developments of numerical methods for DDEs. We are hopeful to report results in this direction in the future.

Other ongoing investigations of the PCF laser concern the role of periodic solutions and their unstable manifolds

in transitions to chaos for larger values of $\kappa\tau$. For a study of the break up of a torus and a subsequent sudden transition to chaos see [18].

In more general terms, we believe that the results presented here showcase the usefulness of continuation and manifold computations for the study of DDEs.

Acknowledgements

The authors thank Koen Engelborghs for his help with DDE-BIFTOOL. B.K. is supported by an EPSRC Advanced Research Fellowship.

[1] G. H. M. van Tartwijk and G. P. Agrawal. Progr. Quantum Electron., **22**, 43 (1998).

[2] B. Krauskopf and D. Lenstra, editors. *Fundamental Issues of Nonlinear Laser Dynamics*, AIP Conference Proceedings, **548** (2000).

[3] A. Gavrielides. In [2], pp 191–217.

[4] J. Mørk, B. Tromborg and J. Mark. IEEE J. Quantum Elec., **28**, 93 (1992).

[5] C. R. Giuliano. Physics Today, pp 27–35, April 1981.

[6] G. R. Gray, D. H. DeTienne and G. P. Agrawal. Opt. Lett., **20**, 1295 (1995).

[7] G. P. Agrawal and G. R. Gray. Phys. Rev. A, **46**, 5890 (1992).

[8] G. H. M. van Tartwijk, H. J. C. van der Linden and D. Lenstra. Opt. Lett., **17**, 1590 (1995).

[9] G. R. Gray, D. Huang, and G. P. Agrawal. Phys. Rev. A, **49**, 2096 (1994).

[10] B. Krauskopf, G. R. Gray, and D. Lenstra. Phys. Rev. E, **58**, 7190 (1998).

[11] X. S. Yao and L. Maleki. Opt. Letters, **22**, 1867 (1997).

[12] T. Heil, I. Fischer, W. Elsässer. J. Mulet and C. R. Mirasso. Phys. Rev. Lett., **86**, 795 (2001).

[13] O. Diekmann, S. A. Gils, S. M. Verduyn Lunel, and H. O. Walther. **110**, (Springer-Verlag, 1995).

[14] J. D. Murray. *Mathematical Biology*, Biomathematics Texts, **19**, (Springer-Verlag, Berlin, 1980).

[15] C. M. Marcus and R. M. Westervelt. Phys. Rev. A, **39**, 347 (1989).

[16] H. Glusing-Luerssen. SIAM J. Control Optim., **35**, 480 (1997).

[17] D. Pieroux, T. Erneux, T. Luzyanina and K. Engelborghs. Phys. Rev. E, **63**, 036211 (2001); D. Pieroux, T. Erneux, B. Haegeman, K. Engelborghs and D. Roose. Phys. Rev. Lett., **87** 193901

[18] K. Green, B. Krauskopf and K. Engelborghs. Bistability and boundary crisis in a semiconductor laser with phase-conjugate feedback. Applied Nonlinear Mathematics Research Report **2002.02**, University of Bristol (2002). `http://www.enm.bris.ac.uk/anm/preprints/2002r02.html`

[19] B. Krauskopf and K. Green. Computing unstable manifolds in delay differential equations. Applied Nonlinear Mathematics Research Report **2002.01**, University of Bristol (2002). `http://www.enm.bris.ac.uk/anm/preprints/2002r01.html`

[20] S. M. Verduyn Lunel and B. Krauskopf. In [2], pp 66–86.

[21] B. Krauskopf, G. H. M. van Tartwijk, and G. R. Gray. Opt. Commun., **177**, 347 (2000).

[22] Y. Kuznetsov. *Elements of Applied Bifurcation Theory* (Springer, Berlin, 1995).

[23] K. Engelborghs, T. Luzyanina, K. in't Hout and D. Roose. SIAM J. Sci. Comput. **22**, 1593 (2000); K. Engelborghs, T. Luzyanina and D. Roose. J. Comput. Appl. Math. **125**, 265 (2000); K. Engelborghs. 'DDE-BIFTOOL', `http://www.cs.kuleuven.ac.be/~koen/delay/ddebiftool.shtml`

[24] G. Samaey, K. Engelborghs and D. Roose. Numerical computation of connecting orbits in delay differential equations. Report **TW 329**, Dept. of Comp. Sci., K. .U. Leuven, Belgium (2001). `http://www.cs.kuleuven.ac.be/publicaties/rapporten/tw/TW329.abs.html`

[25] J. L. A. Dubbeldam, B. Krauskopf and D. Lenstra. Phys. Rev. E, **60**, 6580 (1999).